Background-free volumetric two-photon microscopy by side-lobes-cancelled Bessel beam

Hongsen He, Yu-Xuan Ren, Ryan K. Y. Chan, W. L. So, Hiu Ka Fok, Cora S. W. Lai, Kevin K. Tsia, and Kenneth K. Y. Wong

***Abstract*—We have demonstrated the background-free volumetric two-photon microscopy by cancelling the side lobes of the fundamental 0th-order Bessel beam. The cancellation is based on the fact that the lateral ring patterns of the 3rd-order Bessel beam are well-matched with the side lobes of the 0th-order Bessel beam, so that the image obtained by the 3rd-order Bessel beam is capable to be subtracted as the background of the 0th-order-Bessel-beam-scanned image. We investigated the intensity of the imaging background introduced by the Bessel side lobes under different focusing conditions both in simulations and experiments. The performance of the side-lobes cancellation is showcased on a 50-μm-thick mouse brain slice, and the contrast ratio is enhanced by 2.7 dB for the neurons. This background cancellation technique provides a simple and versatile tool for enhancing the contrast ratio in the two-photon volumetric imaging, especially critical in high-NA cases when a better lateral resolution is pursued.**

***Index Terms*—Bessel beam, side lobes, two-photon microscopy, volumetric imaging, and contrast enhancement.**

I. Introduction

BESSEL beam has been widely applied in the two-photon microscopy (2PM) since it was proved that the axially elongated beam could provide identical lateral resolutions along an extended depth of field (DOF), which allows the rapid volumetric imaging for sparse samples or monitoring neural activities over the entire dendritic spans [1-5]. The most commonly used Bessel beam is the 0th-order Bessel beam, whose lateral intensity distribution is a bright spot in the center and surrounded by a series of concentric rings (side lobes) with decaying intensities [6]. The performance of the Bessel-beam-scanned image is mainly dependent on the excitation of the bright center owing to its dominant intensity, and this is also the reason that the full width of the half-maximum (FWHM) of the bright center is specified as the lateral resolution of the 2PM system [7]. In contrast to the bright center, the side lobes are not only redundant in imaging applications but also contribute greatly to the image background in consequence of their substantially high energies, which degrades the contrast ratio of the image results (supplementary of [2]). The contrast ratio is of great importance in an imaging system, which demonstrates the details distinctly with clearer and sharper edges.

Researchers have attempted several kinds of methods to cancel the side lobes in imaging systems. Kozawa *et al.* demonstrated the effective suppression of the side lobes of a higher-order radially polarized beam by a practical size of the confocal aperture in the conventional laser scanning microscopy [8]. The combination of the three-photon excitation and the Bessel beam was demonstrated to increase the signal-to-background ratio (SBR) in the three-photon microscopy (3PM), benefiting from the higher-order nonlinear effect in the 3PM than that in the 2PM [3, 5]. The axial superposition of two Bessel beams for a main-lobe-only Bessel beam was also investigated in fluorescence microscopes based on interfering the beams of specific wave-vectors [9, 10]. However, the axial pattern alternates between bright and dark regions, which needs to be averaged by several modulated Bessel beams with different axial shifts [9]. Another technique for the side-lobes cancellation is to use a deconvolution method [11, 12]. Although deconvolution is an excellent algorithm for improving image quality, it requires prior information about the structure being imaged. Various values require to be tested for specific images, such as object density, iteration number, and deconvolution mode. Therefore, it is desirable to devise an easy to implement method to reduce the influence of side lobes on the signal of the 0th-order Bessel beam for 2PM, while maintain the DOF.

The image subtraction methods have been extensively investigated for contrast enhancement in imaging systems [13-16]. The implementation of this kind of method is to make a simple subtraction between two images scanned by two beams with different shapes. For example, Yoshida *et al.* utilized the higher-order transverse modes of a cylindrical vector beam for the subtraction [16]. The basic goal of enhancing the contrast ratio for Bessel-beam-scanned images is to keep the main lobe alone while cancel all the side lobes.

This work was supported in part by the Research Grants Council, University Grants Committee (E-HKU701/17HKU C7047-16G, HKU17200219, HKU 17209018), in part by the City University of Hong Kong (CityU T42-103/16-N), and in part by the National Natural Science Foundation of China (61631166003, 61675081, N_HKU712/16). (Corresponding authors: Kenneth K. Y. Wong.)

H. He, Y. X. Ren, R. K. Y. Chan, K. K. Tsia and K. K. Y. Wong are with the Department of Electrical and Electronic Engineering, The University of Hong Kong, Pokfulam Road, Hong Kong, China (e-mail: hshe@connect.hku.hk; yxren@connect.hku.hk; cky166@connect.hku.hk; tsia@eee.hku.hk; kywong @eee.hku.hk).

W. L. So, H. K. Fok and C. S. W. Lai are with the School of Biomedical Science, The University of Hong Kong, Pokfulam Road, Hong Kong, China (e-mail: wls0716@connect.hku.hk; falbert@ hku.hk; coraswl@hku.hk).

Taking advantage of the image subtraction methods, a beam whose lateral profile that can well match the side lobes of the 0th-order Bessel beam is ideal for the subtraction. Fortunately, the higher-order Bessel beams only consist of a series of concentric rings, and the intervals and positions of the rings are also adjustable depending on the Bessel orders [17]. Furthermore, the lateral intensity distributions of all the Bessel beams follow the Bessel function, which means the intensity ratios among the rings are consistent for all the Bessel beams along the radial direction. Therefore, by selecting a Bessel beam with a proper order to obtain the subtraction image, the background of the 0th-order-Bessel-beam-scanned image can be efficiently cancelled.

In this paper, the image scanned by the 3rd-order Bessel beam in the 2PM is used to conduct the subtraction for the 0th-order Bessel beam. The intensity ratio and positions of the side lobes of the 0th-order Bessel beam are well-matched with the ring patterns of the 3rd-order Bessel beam, leading to a sufficient background cancellation. The feasibility of side-lobes cancellation is tested by fluorescent microspheres and the performance of the background-free volumetric 2PM is demonstrated with a mouse brain slice.

I. PRINCIPLES

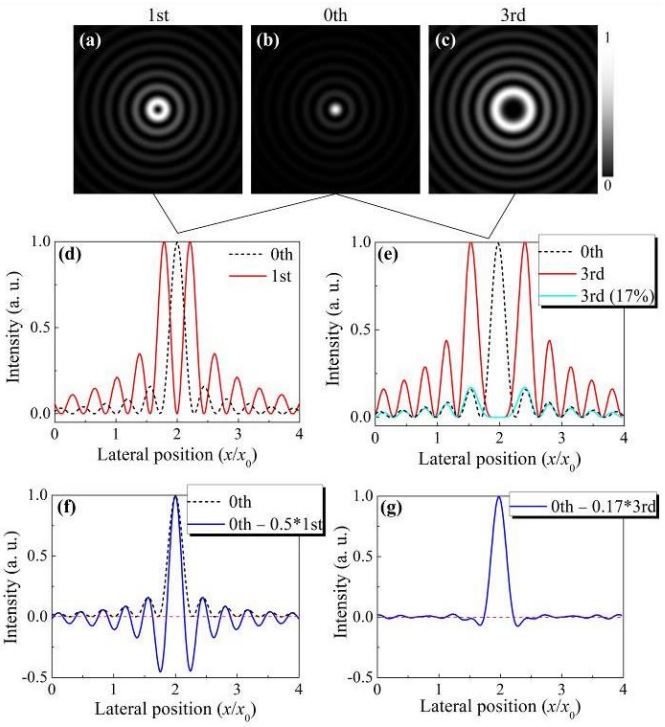

Fig. 1. Simulation of lateral profiles of the 1st-order (a), 0th-order (b), and 3rd-order (c) Bessel beams. (d) Relative lateral profiles of the 0th- and 1st-order Bessel beams. (e) Relative lateral profiles of the 0th- and 3rd-order Bessel beams. (f) Subtracted profile of the 0th- and 1st-order Bessel beams. (g) Subtracted profile of the 0th- and 3rd-order Bessel beams.

The key step for the background subtraction of the volumetric 2PM is to select a high-order Bessel beam with a proper order whose lateral ring distributions are well-matched with the side rings of the 0th-order Bessel beam. The Bessel beam derives from the propagation-invariant solutions of the free-space Helmholtz equation, which has the electric field amplitudes proportional to Bessel functions. The transverse profile of an ideal Bessel beam can be described by [17]

$$E_l(r,\varphi) \propto J_l(k_r r)\exp(il\varphi), \tag{1}$$

where r and φ are the radial and azimuthal components in the cylindrical coordinate, respectively. k_r is the radial wave-vector in the free space. J_l is the lth-order Bessel function of the first kind. Based on Eq. (1), the lateral profiles of the 1st-, 0th-, and 3rd-order Bessel beams are simulated as shown in Figs. 1(a)-1(c), respectively. The 0th-order Bessel beam [Fig. 1(b)] has a bright spot in the center surrounded by a set of concentric rings, while the higher-order ($l \geq 1$) Bessel beams [Figs. 1(a) and 1(c)] consist of concentric rings alone. Moreover, the ring size increases with the Bessel order.

The background cancellation is based on the subtraction between the two images achieved by the 0th- and high-order Bessel beams. The subtracted point spread function (PSF) of the final image is given by [13]

$$PSF_{\text{sub}} = PSF_{\text{0th-Bessel}} - g \cdot PSF_{l\text{th-Bessel}}, \tag{2}$$

where g is the subtraction coefficient. Eq. (2) is the typical subtraction equation for image processing [16, 18, 19]. Based on Eq. (2), our group has demonstrated the resolution enhancement over the extended DOF in volumetric 2PM based on the subtraction of the 0th- and 1st-order Bessel beams [19]. The mechanism is to exploit the smaller dimension of the dark spot of the 1st-order Bessel beams. The relative lateral profiles of the 0th- and 1st-order Bessel beams are shown in Fig. 1(d). The intensity peaks of the 1st-order Bessel beam are all right above the dips of the 0th-order one, which implies the 1st-order Bessel beam is not suitable for the side-lobes cancellation of the 0th-order Bessel beam. The subtraction coefficient is commonly restricted to $0.5 \leqslant g \leqslant 1$ for resolution enhancement [13, 16]. In Fig. 1(f), even a small subtraction coefficient ($g = 0.5$) is chosen, a large negative value (approach to −0.5, whose absolute value is almost half of the maximum image intensity) still occurs in the subtracted image. Furthermore, all the peaks of the side lobes of the 0th-order Bessel beam are still in presence without any intensity reduction, as the comparison of the solid and dashed curves in Fig. 1(f). Therefore, the 1st-order Bessel beam is unable to clean the background efficiently for enhancing the contrast ratio.

By varying the order of the Bessel beam, the 3rd-order Bessel beam is found to be suitable for the background subtraction owing to the fact that its lateral intensity distributions are well-matched with the positions and intensity ratios of the side rings of the 0th-order Bessel beam, as shown in Fig. 1(e). All the peaks of the 3rd-order Bessel beam are right above the corresponding peaks of the 0th-order one, and all the dips are overlapped. By multiplying a proper ratio (17%) of the normalized intensity of the 3rd-order Bessel beam, the new profile almost perfectly covers the side lobes of the 0th-order

Bessel beam, while maintains the main lobe in the center. Fig. 1(g) shows the subtracted profile by the 0th- and 3rd-order Bessel beam. The main lobe of the 0th-order Bessel beam is well maintained, and beyond that the beam intensities approach to zeros, which is similar to a Gaussian profile. It denotes the side-lobes-induced background are cleaned efficiently without over-subtractions.

II. NECESSITY IN TWO-PHOTON MICROSCOPY

The necessity of suppressing the side-lobes of the 0th-order Bessel beam in the 2PM is also analyzed. In two-photon cases, when assuming the sample conditions and temporal intensity distributions of the excitation light are invariant, the fluorescence emitted from a 2D sample can be written as [20]

$$\langle F \rangle \propto \int S^2(r,\varphi)\cdot r dr d\varphi , \tag{3}$$

where $S(r, \varphi)$ is the spatial intensity distribution of the incident beam. In our case, $S(r, \varphi)$ follows the intensity distributions of the Bessel beam, and it also varies under different numerical apertures (NA) of the objective. In the low-NA case, it is sufficient to apply the paraxial approximation on the calculation of the focal electric field, owing to the fact that the focal region of the objective lens is close to the beam axis; while in the high-NA case, considerable portions of the incident wavefront have large refraction angles so that the vectorial nature of light becomes significant. The focal intensity of a Bessel beam under the high-NA objective is given by [21]

$$\begin{aligned} S_{\text{high}}(r,\varphi) \propto & \left[1+\cos\alpha\right]^2 J_0^2(kr\sin\alpha) \\ & +\left[1-\cos\alpha\right]^2 J_2^2(kr\sin\alpha) \\ & +\left[2\sin^2\alpha J_0(kr\sin\alpha) J_2(kr\sin\alpha)\cos 2\varphi\right] \\ & +4J_1^2(kr\sin\alpha)\cos^2\varphi \end{aligned} , \tag{4}$$

where k is the wave vector and equals to $2\pi/\lambda$. λ is the wavelength of the incident beam. α is the maximal half-angle of the cone of light that is focused by the objective. In the low-NA case, α approaches to zero, thus the expression can be simplified as [21]

$$S_{\text{low}}(r,\varphi) \propto J_0^2(kr\sin\alpha) , \tag{5}$$

Both Eqs. (4) and (5) imply that the transverse intensity distributions do not vary with the axial position z. The total two-photon excited fluorescence of the m-th lobe in a lateral plane can be written as [5]

$$\langle F_{\text{m}} \rangle \propto \int_0^{2\pi} \int_{\frac{x_{m-1}}{k\sin\alpha}}^{\frac{x_m}{k\sin\alpha}} S^2(r,\varphi)\cdot r dr d\varphi , \tag{6}$$

where x_{m} is the position of the m-th node (m > 0) of the 0th-order Bessel function. Specifically, $x_0 = 0$, $x_1 \approx 2.4$ and $x_2 \approx 5.5$. To demonstrate the variation of the side-lobes fluorescence, the intensity ratio of the fluorescence between the first lobe (the main lobe) and the second lobe (the first side lobe) is calculated as

$$\text{Ratio} = \frac{\langle F_1 \rangle}{\langle F_2 \rangle} . \tag{7}$$

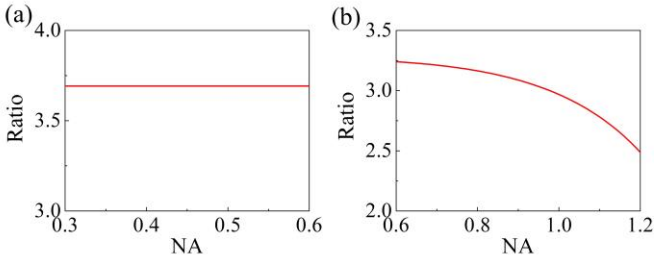

Fig. 2. (a) Simulated fluorescence ratio between the first lobe (the main lobe) and the second lobe (the first side lobe) under low (a) and high (b) NAs of the objective.

The intensity ratio of the fluorescence is calculated under different NAs of the objective, as shown in Figs. 2(a) and 2(b). In the simulations, λ = 1065 nm and NA = $n\cdot\sin\alpha$, where n is the refractive index of the medium between the objective front lens and the specimen. n is set to be 1.33, assuming in the pure water. As shown in Fig. 2(a), the intensity ratio of the fluorescence is constant around 3.7 under low NAs; while it decreases from 3.2 to 2.5 under the NA varying from 0.6 to 1.2 in Fig. 2(b). The gap in Figs. 2(a) and 2(b) at the NA of 0.6 is attributed to the paraxial approximation of Eq. (5). The simulation results show that the side-lobes-induced fluorescence becomes more serious when the Bessel beam is focused by high-NA objectives. Because the high-NA objective is essential in the 2PM for achieving higher spatial resolution, it is necessary to cancel the side lobes of the 0th-order Bessel beam for better image contrast.

III. EXPERIMENTAL SETUP

The experimental setup of the background-free volumetric 2PM is shown in Fig. 3(a). The center wavelength of the excitation laser was at 1065 nm. The laser path was switchable between the Bessel beam and the Gaussian beam. When the Bessel mode was required, M1, M3, and the telescope (L2 and L3) were flipped on. The Bessel beams were generated after the modulation of the SLM (Holoeye, PLUTO) by loading different phase masks. Figs. 3(b) and 3(c) show the intensity distributions of the 0th-order Bessel beam and the 3rd-order Bessel beam, respectively, captured by the CCD camera after the SLM, and the corresponding phase mask is shown underneath. The phase mask for generating the 3rd-order Bessel beam was the superposition of the 3rd-order spiral phase and the axicon phase. A high-NA water-immersion objective (60×, 1.2 NA, UPlanSpo, Olympus) was used to focus the excitation light into the sample. The excited fluorescence signal was collected by a condenser and detected by a PMT (Hamamatsu, H10723-20). Two short-pass filters

(BSP01-785R-25) were used to filter out the residual excitation beam before entering the PMT.

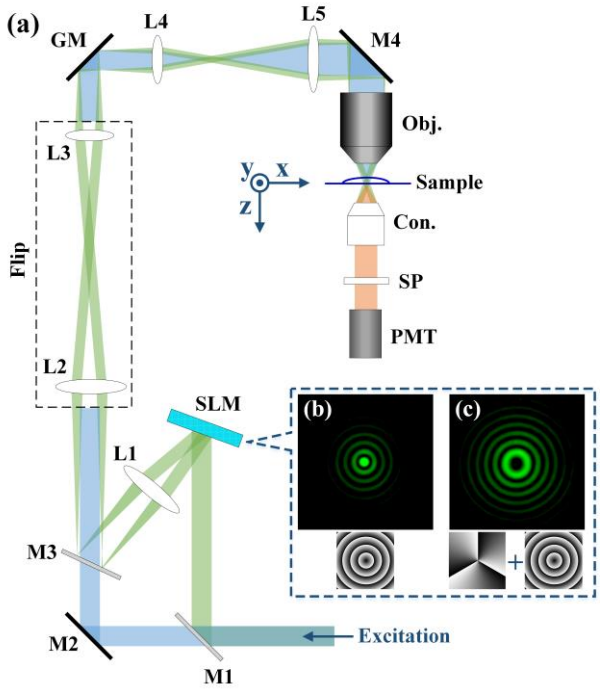

Fig. 3. (a) Experimental setup of the background-free volumetric 2PM. L, lens (L1, focus length f_1 = 150 mm; L2, f_2 = 250 mm; L3, f_3 = 125 mm; L4, f_4 = 80 mm; L5, f_5 = 150 mm). M, mirror. M1 and M3 are capable to be flipped. GM, galvanometric mirror. SLM, spatial light modulator; Obj., objective; Con., condenser; SP, short-pass filter; PMT, photomultiplier tube. (b) (c) Measured beam profiles after the SLM reflection when loading different phase masks.

IV. Results and Discussion

The focusing properties of the Bessel beams under different NAs of the objective were acquired by scanning a 1-μm fluorescent microsphere (F8819, Life Technologies Ltd.). The NA here refers to the effective NA of the objective. By altering the pattern size of the phase mask on the SLM screen, the diameter of the annulus beam (Fourier transform of the Bessel beam) incident on the back aperture of the objective will be adjustable, thus resulting in the variation of the effective NA. The reason of selecting the 1-μm bead is owing to its higher fluorescent signal than smaller ones, which allow us to observe the side lobes more obviously. Though the size of the 1-μm bead is slightly larger than the lateral beam size, the side lobes are still distinguishable [Figs. 4(a1), 4(b1), 4(a2) and 4(b2)]. The peak intensity ratios between the first side lobe and the main lobe of the 0th-order Bessel beam are 3.9% and 6.3% under the effective NA of 0.5 and 0.7, respectively. It shows a much serious influence of the side lobes when the effective NA increases, which agrees with the trend of the integrated intensity ratio of the simulation in Fig. 2. The reason that the integrated intensity ratio is not applied in the experiments is owing to the inhomogeneous intensity distributions of experimental results. Comparing the lateral profiles of the 3rd-order [Figs. 4(b1) and 4(b2)] and the 0th-order [Figs. 4(a1) and 4(a2)] Bessel beams, the annulus sizes of the 3rd-order Bessel beams are always consistent with the side lobes of 0th-order Bessel beams under the same effective NA, contributing to a constantly accordant subtraction. The subtraction coefficients are chosen to be 0.15 and 0.2 under the effective NA of 0.5 and 0.7, respectively. The selection of larger subtraction coefficients than the peak intensity ratios is attributed to the inhomogeneous annulus shapes and imperfectly located concentric rings, where slightly stronger subtraction is capable to compensate the mismatched parts. The brightness of Figs. 4(a1-c2) are enhanced by ×7 to demonstrate the side lobes clearly. In contrast to the 0th-order Bessel beams [Figs. 4(a1) and 4(a2)], the side lobes are eliminated in the subtracted images [Figs. 4(c1) and 4(c2)].

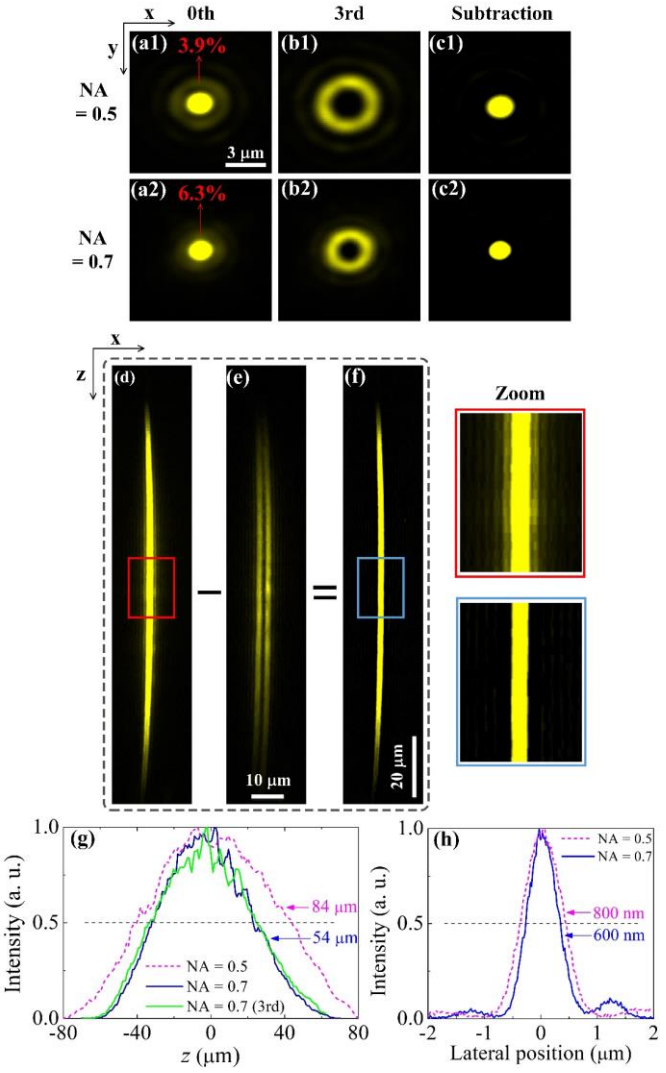

Fig. 4. Intensity distributions of the 0th-order, 3rd-order and subtracted Bessel beams in *x*-*y* plane under the effective objective NA of 0.5 (a1-c1) and 0.7 (a2-c2). Axial intensity distributions of the 0th-order (d), 3rd-order (e) and subtracted (f) Bessel beams in *x*-*z* plane under the effective NA of 0.7. The magnified images correspond to the 0th-order and subtracted Bessel beams. The brightness of (a1-c2, d, f) are enhanced by ×7. (g) Axial lengths of the 0th-order Bessel beam under the effective NA of 0.5 and 0.7, and axial length of the 3rd-order Bessel beam under the effective NA of 0.7. (h) Lateral PSFs of the 0th-order Bessel beam under the effective NA of 0.5 and 0.7.

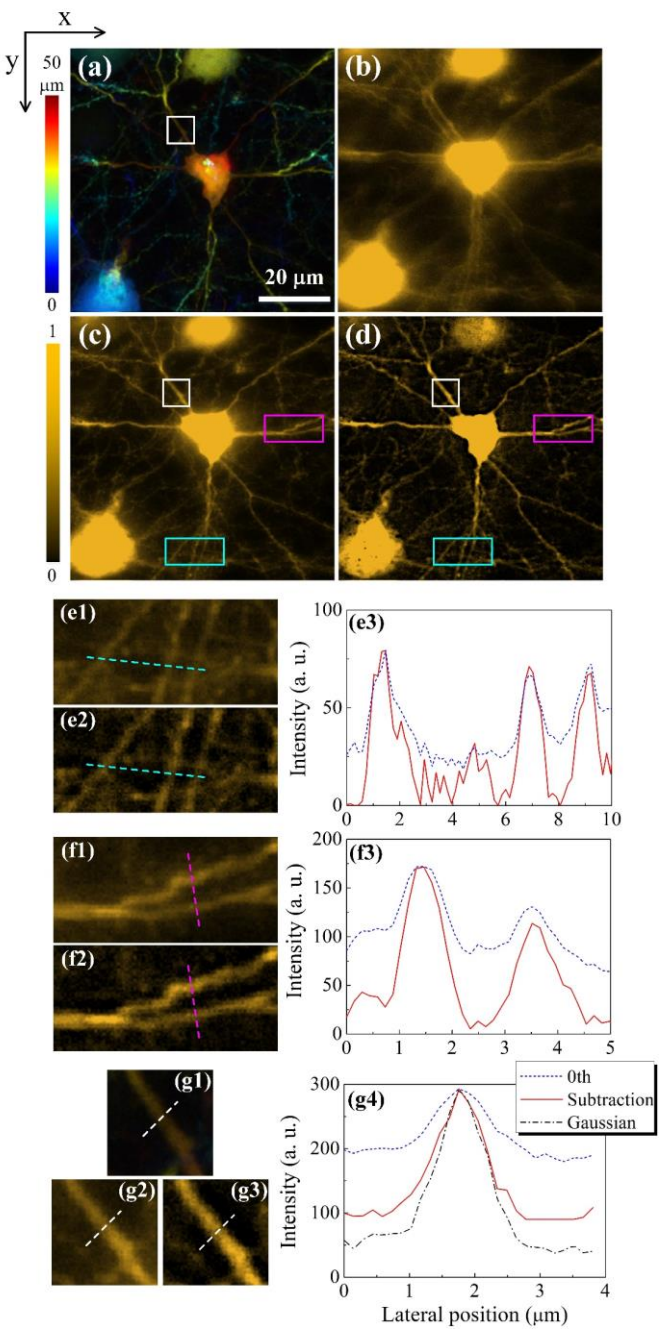

Fig. 5. (a) Projected image along the axial direction of the mouse brain tissue scanned by the Gaussian beam. Images of the same mouse brain tissue scanned by the 3rd-order Bessel beam (b) and the 0th-order Bessel beam (c). (d) Subtracted image between the two images obtained by the 0th- and 3rd-order Bessel beams. Brightness of (b-d): ×7. (e1-e2, f1-f2) Two magnified regions from (c) and (d). (e3, f3) Comparison of the contrast ratios between the 0th-order-Bessel-beam-scanned image and the subtracted image. (g1-g4) Comparison of the contrast ratios of the images obtained by the Gaussian beam (g1), 0th-order Bessel beam (g2), and the subtraction (g3). The post-objective excitation power is ~13 mW for the Gaussian beam, and ~105 mW for the 0th- and 3rd-order Bessel beams.

The 1-μm bead was also scanned along the *z*-axis for obtaining the axial beam profiles for the 0th- and 3rd-order Bessel beams under the effective NA of 0.5 and 0.7. The axial intensity distributions of the 0th-order, 3rd-order, and subtracted Bessel beams under the effective NA of 0.7 are shown in Figs. 4(d-f). The brightness of Figs. 4(d) and 4(f) are enhanced by ×7. The magnified images show the efficient elimination of background induced by the concentric side rings along the radial direction, and only the desired central lobe is maintained over the extended DOF. The axial lengths and lateral PSFs of the Bessel beams under the effective NA of 0.5 and 0.7 are also compared in Figs. 4(g) and 4(h). The nearly equal axial length of the 0th- and 3rd-order Bessel beams at NA = 0.7 ensures the complete subtraction over the extended DOF [Fig. 4(g)]. The lateral PSFs of the Bessel beams were measured by a 100-nm fluorescent microsphere (F8800, Life Technologies Ltd.). By increasing the effective NA of the objective, the beam length decreases from 84 to 54 μm, while the lateral resolution increases from 800 to 600 nm. Given all that, the background subtraction is more critical in high-NA cases when a better lateral resolution is pursued.

As the Bessel beam focused by the higher-NA objective has stronger side lobes that lead to more degradation of the image quality, thick biological tissues were utilized for volumetric imaging to demonstrate the applicability of the background subtraction method. Thus the 0th- and 3rd-order Bessel beams under the effective NA of 0.7 were employed for scanning. The biological sample is a 50-μm-thick mouse brain tissue. The mouse expresses the yellow fluorescent protein (YFP) in a subset of motor and sensory neurons (Thy1-YFP H-line). Layer-V pyramidal neurons in prefrontal cortex were imaged in this paper. All experiments with these samples were approved and performed in accordance with institutional guidelines of the University of Hong Kong. The mouse brain was firstly raster scanned by the Gaussian beam with the axial step of 0.5 μm, and the layer depths are labelled by different colors [Fig. 5(a)]. Then the sample was sequentially scanned by the 0th-order [Fig. 5(c)] and the 3rd-order Bessel beams [Fig. 5(b)], and the subtraction was conducted between these two images, where the image obtained by the 3rd-order Bessel beam aimed to sever as the background [Fig. 5(b)]. The double images for a single neuron in Fig. 5(b) are attributed to the doughnut shape of the 3rd-order Bessel beam. The subtraction coefficient was stepped from 0.2 to 0.6, and 0.5 was identified to be the best one to enhance the image contrast without information loss. The subtracted image is shown in Fig. 5(d). The brightness of Figs. 5(b-d) are enhanced by ×7 to make clear demonstrations of the neurons. In contrast to the image achieved by the 0th-order Bessel beam [Fig. 5(c)], the subtracted image [Fig. 5(d)] maintains all the details of the neuron information with sufficiently subtracted background.

Three imaging regions are magnified from Figs. 5(c) and 5(d) to compare the contrast enhancement performance. In the subtracted images [Figs. 5(e2) and 5(f2)], the neuron profiles are sharper, and the information is all retained. In Figs. 5(e3) and 5(f3), the much higher SBRs in the subtracted images make the intensity peaks of the neurons distinguished better, which are consistent with the appearance of the magnified images. The contrast ratio of the images obtained by the 0th-order Bessel beam [Fig. 5(g2)] and the subtraction [Fig. 5(g3)] are also compared with the Gaussian-scanned results [Fig. 5(g1)]. The three images are magnified from the same regions in Figs. 5(a), 5(c) and 5(d), respectively. The Gaussian curve in Fig.

5(g4) has been multiplied by seven (×7) to make it with the same image brightness as the Bessel images. Here we define the SBR as 10 × log (I_s/I_b), where I_s and I_b are the signal and background intensities, respectively. As shown in Fig. 5(g4), the SBR of the neuron in the subtracted image (4.3 dB) approaches to that from the Gaussian image (6.4 dB), and much higher than the result scanned by the 0th-order Bessel beam (1.6 dB), where the contrast ratio is enhanced by 2.7 dB. It implies the good performance of this background subtraction method with efficient cancellations of the side lobes of the 0th-order Bessel beam.

V. Conclusion

We have demonstrated the background-free volumetric 2PM based on the cancellation of the side lobes of the generally used 0th-order Bessel beam. The excellent cancellation is attributed to the fact that the lateral profile of the 3rd-order Bessel beam is well-matched with the side lobes of the 0th-order Bessel beam, leading to an efficient image subtraction for cleaning the background while avoiding image distortions. Furthermore, the same extended DOF of the two Bessel beams ensures the subtraction is conducted over the whole volumetric region. The application of this method on the mouse brain slice shows good contrast enhancement of the neurons. This background subtraction technique provides a simple and versatile tool for increasing the SBR in the volumetric 2PM, especially for tightly focused modalities.

References

[1] R. Lu, Y. Liang, G. Meng, P. Zhou, K. Svoboda, L. Paninski, and N. Ji, "Rapid mesoscale volumetric imaging of neural activity with synaptic resolution," *Nat. Methods*, vol. 17, no. 3, pp. 291-294, 2020.

[2] R. Lu, W. Sun, Y. Liang, A. Kerlin, J. Bierfeld, J. D. Seelig, D. E. Wilson, B. Scholl, B. Mohar, and M. Tanimoto, "Video-rate volumetric functional imaging of the brain at synaptic resolution," *Nat. Neurosci.*, vol. 20, no. 4, pp. 620-628, 2017.

[3] C. Rodríguez, Y. Liang, R. Lu, and N. Ji, "Three-photon fluorescence microscopy with an axially elongated Bessel focus," *Opt. Lett.*, vol. 43, no. 8, pp. 1914-1917, 2018.

[4] G. Thériault, Y. De Koninck, and N. McCarthy, "Extended depth of field microscopy for rapid volumetric two-photon imaging," *Opt. Express*, vol. 21, no. 8, pp. 10095-10104, 2013.

[5] B. Chen, X. Huang, D. Gou, J. Zeng, G. Chen, M. Pang, Y. Hu, Z. Zhao, Y. Zhang, and Z. Zhou, "Rapid volumetric imaging with Bessel-Beam three-photon microscopy," *Biomed. Opt. Express*, vol. 9, no. 4, pp. 1992-2000, 2018.

[6] D. McGloin, and K. Dholakia, "Bessel beams: diffraction in a new light," *Contemp. Phys.*, vol. 46, no. 1, pp. 15-28, 2005.

[7] L. Thibon, L. E. Lorenzo, M. Piché, and Y. De Koninck, "Resolution enhancement in confocal microscopy using Bessel-Gauss beams," *Opt. Express*, vol. 25, no. 3, pp. 2162-2177, 2017.

[8] Y. Kozawa, T. Hibi, A. Sato, H. Horanai, M. Kurihara, N. Hashimoto, H. Yokoyama, T. Nemoto, and S. Sato, "Lateral resolution enhancement of laser scanning microscopy by a higher-order radially polarized mode beam," *Opt. Express*, vol. 19, no. 17, pp. 15947-15954, 2011.

[9] X. Hua, C. Guo, J. Wang, D. Kim-Holzapfel, B. Schroeder, W. Liu, J. Yuan, J. French, and S. Jia, "Depth-extended, high-resolution fluorescence microscopy: whole-cell imaging with double-ring phase (DRiP) modulation," *Biomed. Opt. Express*, vol. 10, no. 1, pp. 204-214, 2019.

[10] G. Di Domenico, G. Ruocco, C. Colosi, E. DelRe, and G. Antonacci, "Cancellation of Bessel beam side lobes for high-contrast light sheet microscopy," *Sci. Rep.*, vol. 8, no. 1, pp. 1-7, 2018.

[11] B. Jiang, X. Yang, and Q. Luo, "Reflection-mode Bessel-beam photoacoustic microscopy for in vivo imaging of cerebral capillaries," *Opt. Express*, vol. 24, no. 18, pp. 20167-20176, 2016.

[12] J.-B. Sibarita, "Deconvolution microscopy," *Microscopy Techniques*, pp. 201-243: Springer, 2005.

[13] H. Dehez, M. Piché, and Y. De Koninck, "Resolution and contrast enhancement in laser scanning microscopy using dark beam imaging," *Opt. Express*, vol. 21, no. 13, pp. 15912-15925, 2013.

[14] K. Korobchevskaya, C. Peres, Z. Li, A. Antipov, C. J. Sheppard, A. Diaspro, and P. Bianchini, "Intensity weighted subtraction microscopy approach for image contrast and resolution enhancement," *Sci. Rep.*, vol. 6, pp. 25816, 2016.

[15] A. Gasecka, A. Daradich, H. Dehez, M. Piché, and D. Côté, "Resolution and contrast enhancement in coherent anti-Stokes Raman-scattering microscopy," *Opt. Lett.*, vol. 38, no. 21, pp. 4510-4513, 2013.

[16] M. Yoshida, Y. Kozawa, and S. Sato, "Subtraction imaging by the combination of higher-order vector beams for enhanced spatial resolution," *Opt. Lett.*, vol. 44, no. 4, pp. 883-886, 2019.

[17] J. Arlt, and K. Dholakia, "Generation of high-order Bessel beams by use of an axicon," *Opt. Commun.*, vol. 177, no. 1-6, pp. 297-301, 2000.

[18] S. Segawa, Y. Kozawa, and S. Sato, "Resolution enhancement of confocal microscopy by subtraction method with vector beams," *Opt. Lett.*, vol. 39, no. 11, pp. 3118-3121, 2014.

[19] H. He, C. Kong, K. Y. Chan, W. So, H. K. Fok, Y.-X. Ren, C. S. Lai, K. K. Tsia, and K. K. Wong, "Resolution enhancement in an extended depth of field for volumetric two-photon microscopy," *Opt. Lett.*, vol. 45, no. 11, pp. 3054-3057, 2020.

[20] C. Xu, and W. W. Webb, "Multiphoton excitation of molecular fluorophores and nonlinear laser microscopy," *Top. Fluoresc. Spectrosc.*, pp. 471-540: Springer, 2002.

[21] E. Botcherby, R. Juškaitis, and T. Wilson, "Scanning two photon fluorescence microscopy with extended depth of field," *Opt. Commun.*, vol. 268, no. 2, pp. 253-260, 2006.